Efficient Programmable Pulse Shaping for X-band GaN MMIC Radar Power Amplifiers

C. Florian, *Member, IEEE*, T. Cappello, *Student Member, IEEE*, D. Niessen, *Member, IEEE*, R. P. Paganelli, S. Schafer, *Student Member*, IEEE, and Z. Popovic, *Fellow, IEEE*

***Abstract*— This paper presents a supply-modulated X-band 12-W peak power transmitter that maintains an average efficiency greater than 50% for various shapes of amplitude-modulated pulses. The main PA is a two-stage GaN-on-SiC MMIC with a peak efficiency of 65%, while the pulse envelope modulator is a 95% efficient hybrid 3-bit power DAC implemented with GaN-on-Si transistor switches. Envelope shaping of a pulsed waveform results in improved spectral confinement of greater than 15 dB for the first sideband compared to constant-envelope pulses, with over 20 points improvement in total efficiency. The combination of supply modulation (SM) and digital pre-distortion (DPD) is shown to result in high composite (total) efficiency of over 55%, with simultaneous high dynamic range and with flexible digitally-programmable pulse shaping.**

***Index Terms*—Radar pulse shaping, spectral confinement, supply modulator, envelope tracking (ET), power DAC.**

I. Introduction

The majority of radar systems operate the high power amplifier (PA) of the transmitter in pulsed regime: the characteristics of the RF/microwave pulses in terms of duty cycle, pulse width, repetition frequency, transmitted power and pulse shaping directly affect radar performance [1]. Solid-state phased array radar are enabled by a large number of transmit modules that produce very high transmit powers. A typical transmit module has an efficient nonlinear deep class AB to class-C power amplifier (PA) that transmits constant-envelope pulses with significant spectral content over a large bandwidth [1]. Advanced radar waveforms can be used to provide spectral confinement, improve range ambiguity and decrease detectability for Active Electronically Scanned Arrays (AESA) [2]. In search and tracking radar, target detection and identity discrimination can be improved [3], while in weather radar suppression of transmitted spectral sidebands enhances performance [4]. Additionally, there is increased concern about radar spectral emissions interfering with communication spectrum allocations [5].

Amplitude modulation of the envelope provides spectral confinement effects on radar system performance for different envelope shapes ~~e.g.~~ [1]-[7]. The amplitude-modulated pulse can be provided at the input of the PA while the supply voltage is kept constant over the pulse duration. Such drive-modulated PAs operate in back-off at lower amplitudes, resulting in significant average efficiency degradation. In [6], [7] an out-phasing PA with a Gaussian envelope shape, with up to a 3-dB peak-to-average ratio (PAR) waveform is experimentally investigated, but the average system efficiency is not reported.

C. Florian, T. Cappello, D. Niessen are with the Department of Electrical, Electronic and Information Engineering of the University of Bologna, Bologna, 40136, Italy. (E-mail: corrado.florian@unibo.it). R.P. Paganelli is with the National Research Council, CNR-IEIIT, Bologna, Italy. Scott Schafer and Zoya Popovic are with the Department of Electrical, Computer and Energy Engineering, University of Colorado at Boulder, Boulder CO, USA.

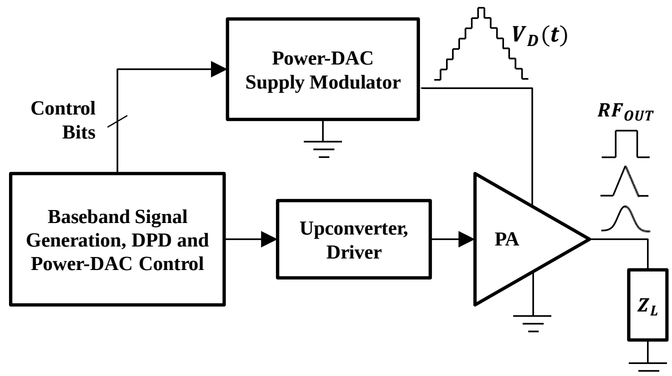

Fig. 1. High-level block diagram of the radar transmitter with a power DAC (pDAC) supply modulator. The digital baseband signal processing provides the signal that is upconverted and drive-modulates the PA, as well as the control bits for the pDAC. The pDAC is implemented with GaN-on-Si power devices, while the PA is a GaN-on-SiC MMIC. The digital signal processing includes predistortion.

More recently, supply modulation (SM) was introduced as a means to amplify amplitude-modulated pulses without sacrificing PA efficiency [8]-[16]. Various types of supply modulation following up on the early envelope elimination and restoration (EER) technique [17] have been applied to improve efficiency of transmitters for high peak to average power ratio (PAPR) communication signals ~~[8-13]~~. In [2] a PWM 100-MHz switching converter is used for linear pulse shaping of an integrated S-band PA, with a total efficiency of 27%. For pulse-shaping of a hybrid S-band GaN PA in [14], a variable supply [15] is implemented as a simple damped resonant circuit with efficiency greater than 90% at 6 W output power and a total efficiency 50% and greater than 65% for PAPR values of 8 and 4dB, respectively. An average 66% total efficiency was demonstrated for a Blackman-window pulse with a 4.1-dB PAPR and -30 dB spectral sidelobe levels. In [15], [16], this method was applied to X-band GaN PAs with variable 7-15 μsec pulse widths and a resulting efficiency of 40%. For good sideband suppression, simple predistortion of the PA gain and phase was required in this approach. Although good efficiency improvement and spectral confinement was demonstrated, the drawback of the technique is that it is limited to a single pulse shape due to the resonant nature of the supply.

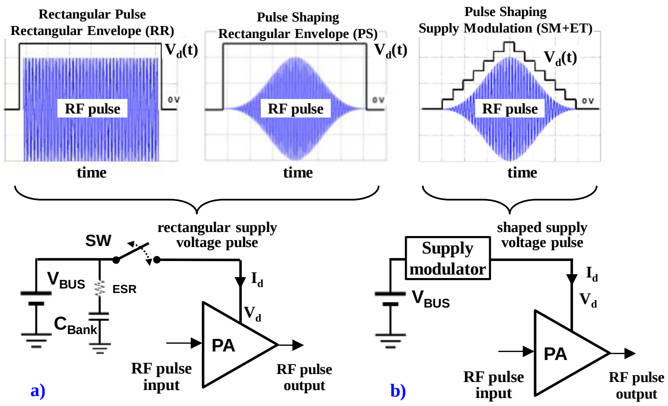

Fig. 2. (a) Pulse waveforms and circuit diagram for constant supply case. (b) Amplitude-modulated pulse waveform with discretized envelope and associated circuit architecture.

In this paper, we extend the supply pulse shaping technique to a fully programmable discrete-level supply which modulates an efficient 12-W GaN MMIC X-band PA, as illustrated in Fig.1. In this approach, the digital baseband signal is generated and pre-distorted in an FPGA and upconverted to drive-modulate the GaN-on-SiC 10-GHz MMIC PA. The FPGA also provides control bits for a 3-bit power DAC (pDAC) multi-level dynamic supply, implemented with GaN-on-Si power devices. The pulse shape is fully programmable and can provide not only amplitude modulation of each pulse, but also pulse-to-pulse modulation.

In the work presented here, and in contrast to linear tracking such as described in [2], the pDAC discretizes the envelope in steps and the linearity is recovered by DPD of the RF PA. The switches of the pDAC commutate at only a few kHz, and the nonlinearities are compensated with DPD, allowing for large efficiency increase to over 55% at X-band.

The multilevel power converter (pDAC) used here as the supply modulator of a radar transmitter was first introduced in [24] for the implementation of an envelope tracking transmitter at L-band for LTE communication signals with an hybrid LDMOS PA. Here, the pDAC is used as a part of an X-band radar transmitter based on a GaN MMIC PA. The exploitation of the pDAC for this new application enables the synthesis of arbitrary, digitally-programmable radar pulse envelope shaping, while maintaining very high composite efficiency. This type of transmitter enables other useful operating modes such as pulse-width modulation and pulse-to-pulse modulation.

The remainder of this paper presents the transmitter architecture and measurement setup, detailed in Section II, followed by a brief description of the pDAC multi-level supply modulator and required pre-distortion in Section III. Section IV presents the design and characterization of the MMIC PA at X-band. In Section V, the results of the transmitter measurements with the pDAC connected to the MMIC PA show that high average overall efficiency can be obtained with simultaneous high dynamic range and spectral confinement. Section VI presents ~~some conclusions and~~ a discussion of other relevant capabilities of this architecture, such as pulse-width modulation and pulse-to-pulse modulation.

II. Transmitter Architecture and Measurement Setup

A common configuration for the power supply of a radar transmitter is illustrated in Fig. 2a. The supply voltage V_d of the RF PA is provided by switching on/off the system bus voltage supply V_{BUS}, which is typically generated by a switching power supply. A power switch (SW in Fig. 2a) is connected in series between V_{BUS} and the PA bias pad, and a bank of high-Q capacitors (C_{BANK}) is designed to guarantee a limited roll-off of V_d and delivers the PA supply current (I_d) during the pulse. This type of operation is standard for X and C-band GaAs and GaN MMIC PAs described in [18]-[20]. The PA operates always at peak PAE deep in gain compression and the strong nonlinearities in addition to rectangular pulse spectral spreading generate significant sidebands in the transmitted radar spectrum. When a Gaussian-type pulse is applied to reduce the spectral-domain sidebands, if the supply is kept constant (PS case in the upper part of Fig. 2), the efficiency of the PA is greatly reduced.

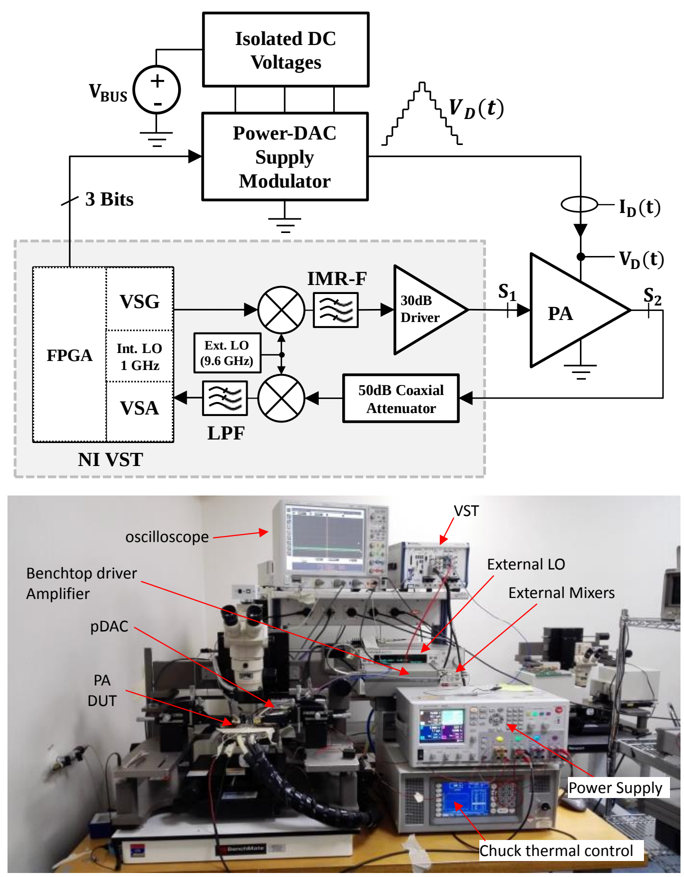

Fig. 3. Block diagram of setup and picture for radar transmitter pulse shaping measurements. Three isolated DC voltages are input to the pDAC which is controlled from the FPGA in the NI VST 5644R. The mixers are commercial Minicircuits devices, and the image-rejection (IMR-F) and low-pass filter are specifically designed for this setup.

Fig. 2b shows the alternate approach when the same shaping of the RF pulse envelope is also applied through the supply. Here, a supply modulator is used between the system voltage bus and the PA and dynamically maintains the PA at high efficiency by supply modulation (SM).

The supply amplitude-modulated transmitter system setup is illustrated in more detail in Fig. 3, along with a photograph of the laboratory set-up. The vector signal generator and analyzer is a National Instrument PXIe-5644R VST, which is an FPGA-based instrument used for the generation and analysis of arbitrary digital modulated RF signals, with an analog bandwidth of 80 MHz. The signal is generated in digital baseband and upconverted first to 1 GHz directly within the VST. A second upconversion stage to X band is performed with a double-balanced diode mixer (Minicircuits ZX05-153MH-S+) and after filtering, amplification is provided by an instrumentation amplifier (Agilent 83020A). Note that any type of digital vector modulation can be applied to the baseband signal prior to up-conversion.

In the receiver section, the RF signal is down-converted twice, sampled and then analyzed in the time domain. At the PA output, the signal is attenuated (50 dB coaxial attenuator), down-converted to 1 GHz by a second mixer, and low-pass filtered before the VST input port. A microstrip image-rejection filter (IMR-F) in the up-conversion chain and a coaxial low-pass filter in the down-conversion chain were designed in-house. The external LO (Agilent 83650B) is locked to the same low-frequency reference clock as the internal LO of the VST. The VST stores the I/Q data of the RF signal at the DUT input and output, while the modulated supply voltage $V_d(t)$ and currents $I_d(t)$ of the PA (Fig. 3) are acquired by a digital oscilloscope equipped with wideband voltage and current sensors. The set-up is calibrated at the DUT input and output ports, S_1 and S_2 in Fig. 3, corresponding to the GSG probe tips connected at the input and output port of the MMIC PA.

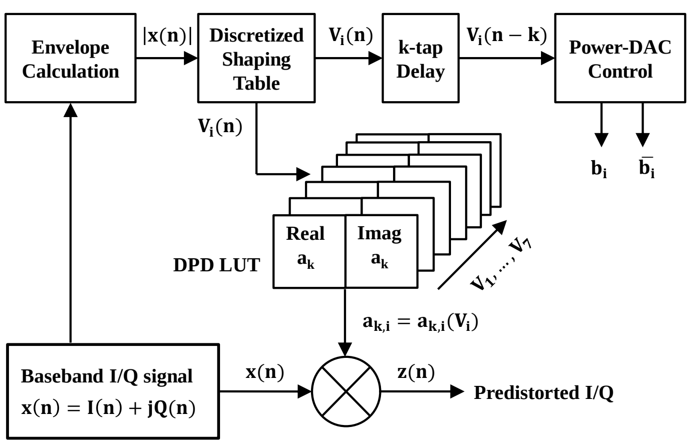

Fig. 4. Generation of the predistorted I/Q and of the pDAC commands in firmware loaded in the FPGA. The top branch shows the envelope signal generation for pDAC control, while the bottom branch describes the generation of the pre-distorted signal, which is input to a DAC before upconversion.

The modulation and DPD associated with a specific pulse shape is implemented in firmware (LabVIEW FPGA VI) and loaded in the instrument FPGA. The firmware also generates digital commands for control of the dynamic bias supply, by comparing the RF signal envelope with the PA bias supply-shaping table, which consists of the optimum supply voltage V_d trajectory for PAE maximization [13]. The firmware also regulates time alignment between RF drive and supply modulation paths, which is fundamental to correct SM operation. The FPGA is clocked at 120 MHz, and the control/baseband signal time step is 4.16 ns, due to internal fractional interpolation. The signal flow through the test setup can be summarized as follows, referring to Fig. 4:

1) the I/Q signals of the arbitrary shaped pulsed RF waveform *x(n)* are generated in the VST and their corresponding envelope |*x(n)*| is calculated in the FPGA;

2) V_i voltage level is selected based on the calculated envelope that maximizes the PAE, according to the PA discretized supply shaping function $V_i = \mathcal{F}_D\left(|x(n)|\right)$ stored in a LUT in the FPGA. The corresponding digital commands b_i are generated for the pDAC;

3) the value of V_i dictates the complex DPD coefficients $a_{k,i}$ to compensate AM/AM and AM/PM characteristics of the PA at supply level V_i.

4) the DPD coefficients are applied to the input signal to generate the predistorted I/Q, which is then upconverted and input to the PA input, synchronously with the corresponding supply commands b_i.

Referring to Fig. 4, the coefficients $a_{k,i}$ of the seven polynomials corresponding to the seven levels V_i are stored in eight different LUTs. This implementation of the DPD function with multiple LUTs avoids some of the discontinuity problems that could arise with a single predistorter function covering the entire dynamic range of the PA.

The DPD strategy implemented in the setup is in open loop, since there is no adaptation of the DPD coefficients at runtime. However, since the DPD LUTs are implemented in the FPGA of the same instrument that contains the receiver (Fig. 3), a closed-loop DPD can also be implemented, by synthesizing an adaptation algorithm for the DPD coefficients in the FPGA firmware. Such an implementation could be useful to track temperature or aging variations of the PA, or to implement a memory DPD required for higher bandwidth operation (*e.g.* for wideband radar pulses with pulse widths lower than 1 μs). For the experiments reported in this paper, with a fixed baseplate temperature (T_B = 60), relative short observation time and pulse widths in the 1-100 μs range, the memoryless open-loop approach is shown to be sufficient, as will be seen from the measured system-level results in Section V.

III. Power-DAC Supply Modulator and DPD

Multi-level dynamic power supplies demonstrated efficiency improvements in, e.g. outphasing transmitters [21]-[23]. Typically, one of 4 supply voltage levels is switched in for a time period that depends on signal statistics. In this paper, a different type of multi-level supply is used and we refer to it as a pDAC because 3 supply voltages can be combined to give 2^3=8 voltage levels. Because of the discrete nature of the supply modulation, predistortion of the signal becomes a necessity. In this section, the architecture of the pDAC described in detail in [24] is reviewed for completeness, followed by a description of the DPD required for amplitude-modulated radar pulses.

A. Power DAC Supply Modulator

The pDAC shown in Fig. 5 is demonstrated in [24] to effectively modulate an ET hybrid LDMOS S-band PA with 10-MHz LTE and WiFi high PAPR signals. The pDAC features a full power bandwidth larger than 20 MHz and a spurious free dynamic range of about 26.5 dB (measured at 1 MHz).

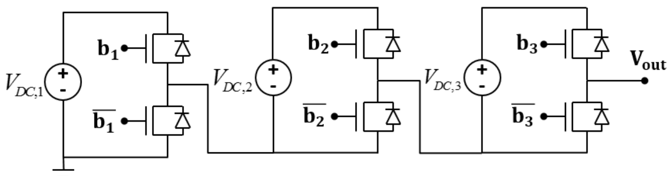

Fig. 5. 3-level pDAC topology with binary-weighted isolated voltage sources.

The modulator is capable of sweeping through its entire voltage dynamic range of 42 V in far less than 1 µs and is thus suitable for tracking the envelope of amplitude-modulated pulsed signals, which are typically 1 to 100 µs wide in radar applications, The corresponding $V_d(t)$ profile shown in Fig. 2b has a discrete staircase shape, produced by the pDAC circuit shown in Fig. 5, composed of three cascaded half-bridge converters, which control three isolated voltage sources ($V_{DC,1}$, $V_{DC,2}$, $V_{DC,3}$). This converter topology can implement the binary-coded sum of the input voltage sources, with an output waveform resolution of (2^N-1) levels, compared to N for a standard multilevel converter. The converter output voltage V_{out} is a binary-coded 8-level step waveform (one level is zero) given by,

$$V_{out} = \sum_{i=1}^{3} b_i V_{DC,i} \quad \text{with} \quad V_{out}^{MAX} = V_{DC,1} + V_{DC,2} + V_{DC,3} \tag{1}$$

where b_i is the binary (b_i = 1, 0) controlling command of the *i-th* half bridge cell, generated by the FPGA in Fig. 4. Compared to the common ET approach that combines a PWM switching Buck converter with a linear amplifier, the pDAC has advantages in terms of dynamic range, full power bandwidth and efficiency. The drawback is the limited resolution of the output waveform, which introduces a discretization error in the dynamic supply voltage ($V_{out}(t)$ = $V_d(t)$), that will also be observed in the PA output signal as distortion. Nonetheless, due to the relatively large number of voltage levels provided by this pDAC topology the discretization error is limited, and can be compensated by digital pre-distortion (DPD) of the RF signal. It is worth noting that the topology of Fig. 6 is modular, and a pDAC with a higher number of bits can be implemented, resulting in finer discretization of the synthesized dynamic supply voltage $V_d(t)$. This would increase the average PA efficiency at the expense of an increased number of commutations of the power switches of the pDAC, thus at lower pDAC efficiency. Given this trade-off for the optimization of the overall transmitter efficiency, a 3-bit implementation of the pDAC represents a good compromise, since seven V_d levels are enough to supply-modulate a PA with a substantial increase of its operating PAE, while maintaining the pDAC efficiency very high.

B. Digital Pre-Distortion (DPD) for Pulse Shaping

The predistorter for the linearization of the PA working under SM operation is implemented in open loop with a memoryless polynomial model defined by

$$z(n) = \sum_{k=1}^{K_i} a_{k,i}\, x(n) \left| x(n) \right|^{k-1} \tag{2}$$

$$a_{k,i} = \left| a_{k,i} \right| e^{j\angle a_{k,i}} = a_{k,i}(V_i) \qquad i = 1 \ldots N \tag{3}$$

$$V_i = \mathcal{F}_D\left(\left| x(n) \right| \right) \qquad i = 1 \ldots N \tag{4}$$

where $x(n)$ is the baseband signal at the PA input before DPD and $z(n)$ is the baseband predistorter output. The complex polynomial coefficients $a_{k,i}$ depend on the instantaneous supply voltage V_i, where the V_i's are selected by the input signal amplitude $|x(n)|$, according to the discretized shaping function $\mathcal{F}_D$. The model coefficients are identified by complex polynomial fitting of the inverse of the PA AM/AM and AM/PM characteristics, with some off-line coefficient optimization, as shown in the next section. Least-squares fitting of seven complex polynomials, one polynomial for each level V_i, to the measured characteristics is performed.

IV. PA Characterization for Discrete-Level Supply Modulation

The PA is a two-stage MMIC implemented in the Qorvo 0.15-µm GaN-on-SiC HEMT technology.

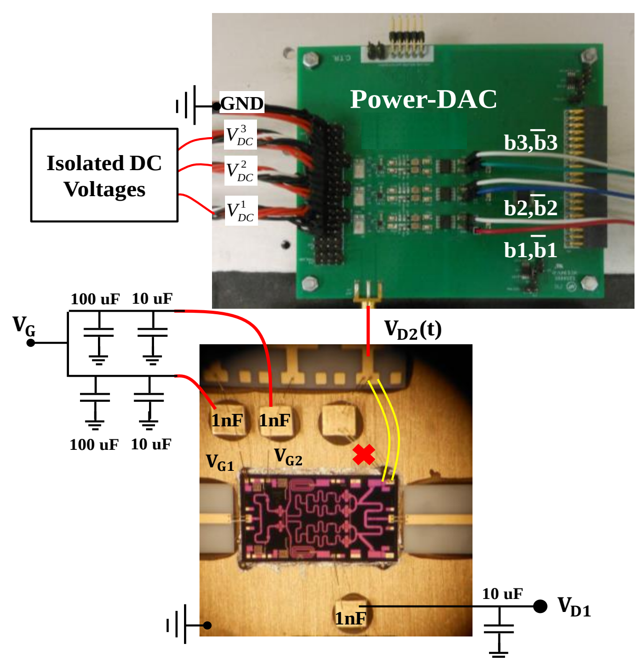

Fig. 6. Photographs of the pDAC board and MMIC PA, with a sketch of the connections of the PA to supplies and to the pDAC. The drain of the second stage amplifier has been directly bonded to the carrier pad.

A similar PA designed in the same process is reported in [25] for tracking OFDM signals with an inefficient linear supply.

The MMIC PA integrated with the pDAC and shown in Fig.6 is reported here for the first time and is designed for supply modulation with peak efficiency somewhat below the highest level of 20 he PA is designed to be stable with no external capacitors on the bias network, since the drain bias network needs to pass broadband signals from the dynamic supply. The first driver stage of the PA is composed of two 8x50 µm devices, while four 10x90 µm devices are combined in the second stage, with an gain greater than 20dB at 2-3 dB gain compression. The maximum drain supply voltage is V_D = 20 V, for a total class-AB quiescent drain current I_D = 325 mA (55 mA for the first stage, 270 mA for the second stage).

As seen in Fig. 6, only the second stage of the PA is modulated by the pDAC, while the drain voltage of the first stage is kept fixed at V_{d1} = 20 V. Fig. 6 shows the connections between the PA and the pDAC, along with the other drain and gate bias networks. While for V_{G1}, V_{G2} and V_{d1} bias connections, off-chip bypass capacitors are added to ensure PA stability, no external capacitance is added to the second stage drain pad V_{d2} in order to enable fast modulation of this supply voltage. The only bypass capacitance to this node is provided by the on-chip integrated MIM (Metal-Insulator-Metal) capacitors, for a total value of 30 pF. The connection between the supply modulator and the PA is kept as short as possible for a total estimated inductance of about 30 nH. The PA is soldered on a large CuMo carrier and the input/output RF pads are accessed with GSG microprobes through short 50-Ω microstrip lines on alumina, wire-bonded to the MMIC RF pads. The PA frequency sweep shows a bandwidth from about 9 to 10.5 GHz, with peak efficiency at 9.6 GHz.

The PA was characterized in the setup of Fig. 3 to identify the supply shaping table and the complex polynomial for the DPD. Fig. 7 shows the measured output power at 9.6 GHz versus available source power over a range of final stage drain voltages. The 0-20 V drain voltage interval was discretized with the voltage levels V_i shown in the inset of Fig. 7, synthesized by the pDAC as binary sums of the input voltages

$$V_{DC,1} = 11.2\ \text{V},\ V_{DC,2} = 5.6\ \text{V},\ V_{DC,3} = 3.2\ \text{V}.$$

The measurement results in Fig. 7 to Fig. 9 are performed with a pulse width of 50 µs with 10% duty cycle, which are typical values for many types of pulse-compressed radar transmitters (e.g. the ones in [18]-[20]). The AM/AM and AM/PM characterization of the PA is carried out with an amplitude modulated RF pulse, sweeping the entire PA dynamic range for each supply voltage V_i. With this setup, the PA characterization at different supply voltages is carried out in pulsed regime, under thermal conditions very similar to the operating ones.

In Fig. 7 and 8, the measured output power and available power gain of the PA are shown for the different pulsed drain supply as $V_d = V_i$. The measured PAE is shown in Fig. 9 where power consumption is calculated from the measured instantaneous values of $V_d(t)$ and $I_d(t)$.

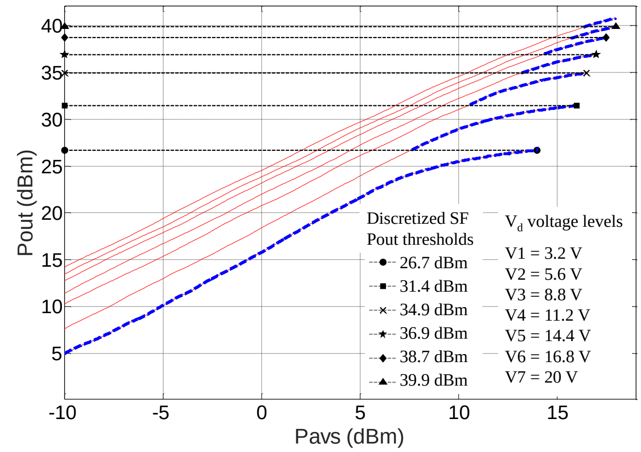

Fig. 7. Measured PA output power for different $V_d = V_i$ at 9.6 GHz and a gate bias of $V_{G1} = V_{G2}$ = -2.7 V for both stages. The dashed bold lines represent the SM trajectory followed with the selected supply shaping function. In the inset, the selected discretized supply shaping function is listed as a function of the output power.

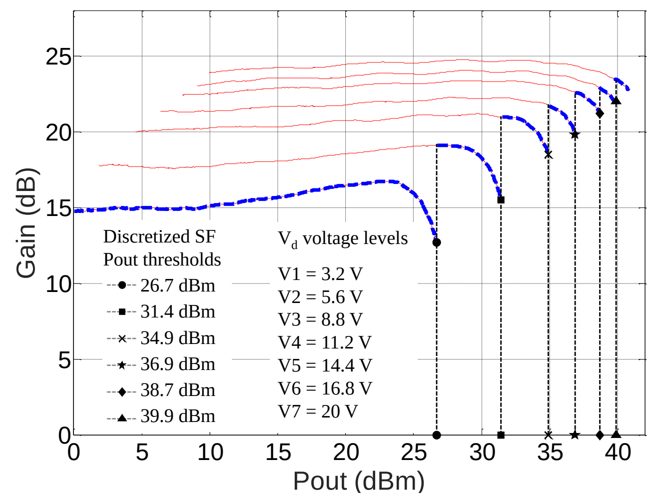

Fig. 8. Measured PA gain at 9.6 GHz for different $V_d = V_i$. The dashed bold lines represent the SM trajectory followed with the selected supply shaping function. In the inset, the selected discretized supply shaping function is listed as a function of the output power.

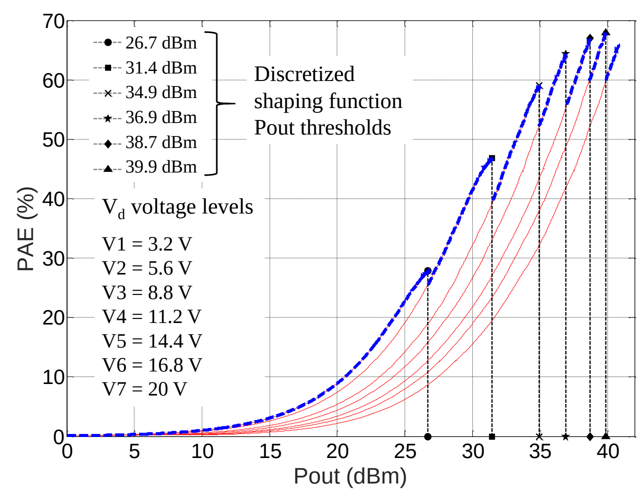

Fig. 9. Measured PA PAE at 9.6 GHz for different $V_d = V_i$. The dashed bold lines represent the SM trajectory followed with selected supply shaping function. In the text inset, the selected discretized supply shaping function is listed as a function of the output power.

The peak PAE was not reached for the highest voltage levels, due to power limitation of the instrumentation amplifier driver, however the PA is in more than 2 dB of gain compression even at the V_d = 20 V level, as shown in Fig. 8. This characterization shows the following PA peak performance at V_d = 20 V: P_{out} = 40.7 dBm, *Gain* = 23 dB and PAE = 65%.

The selected supply shaping function is represented by the P_{out}, *PAE* and gain trajectories highlighted with the dashed bold lines in Figs. 7, 8 and 9. The symbols in the graphs indicate the P_{out} thresholds for V_d level commutation of the discretized shaping table, which is a simple two-column LUT (output or input power *vs.* V_d) stored in the FPGA of the instrument. The shaping table is listed in the text insets of Figs. 7 to 9. In Fig. 8, the relevant gain variation associated with the selected supply shaping table is shown: this variation (from 15 dB for V_d = 3.2 V to 23 dB for V_d = 20 V) is due to the variation of the quiescent drain current (I_{D2} = 48 mA for V_d = 3.2 V, I_{D2} = 270 mA for V_d = 20 V) and the corresponding change of the input/output impedances, and thus matching characteristics, of the devices in the PA final stage.

The gain steps corresponding to different supply levels and the gain variation within each level need to be compensated by the predistorter, which is designed to linearize the SM PA characteristic to a constant compressed gain of 23 dB, at the maximum output power (V_d = 20 V at maximum input power).

Since the PA gain decreases significantly with lower supply voltages (Fig. 8), the predistorter gain needs to provide significant gain expansions to obtain the target constant transmitter gain of 23 dB.

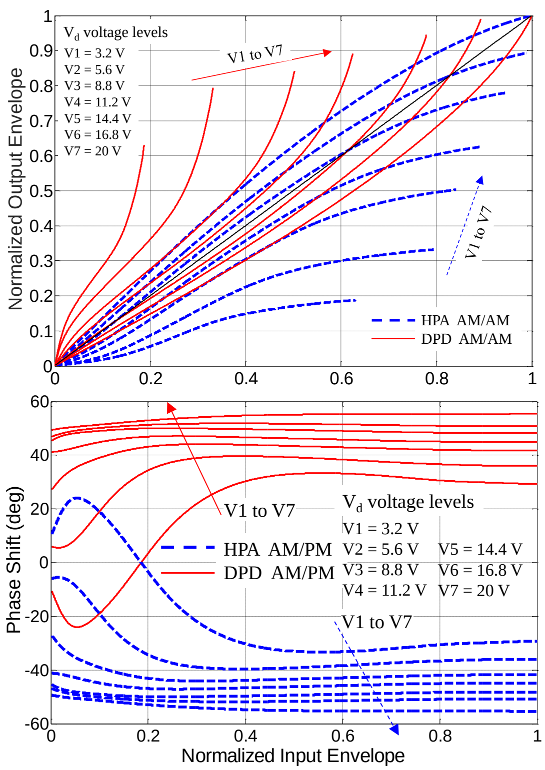

Fig. 10. PA and predistorter AM/AM (upper) and AM/PM (lower) characteristics for each supply voltage level.

In Fig. 10, the predistorter amplitude and phase characteristics for each voltage level are shown (solid lines), along with the PA AM/AM and AM/PM behavior (dashed bold lines). The DPD amplitude expansion needed for the linearization of the PA gain compression is evident in these plots.

The same information in time domain can be seen in Fig. 11, where the ideal envelope of the RF input signal (dashed bold line) for pulse shaping with a Blackman window is shown along with the actual pre-distorted envelope for the SM PA linearization (solid thin line).

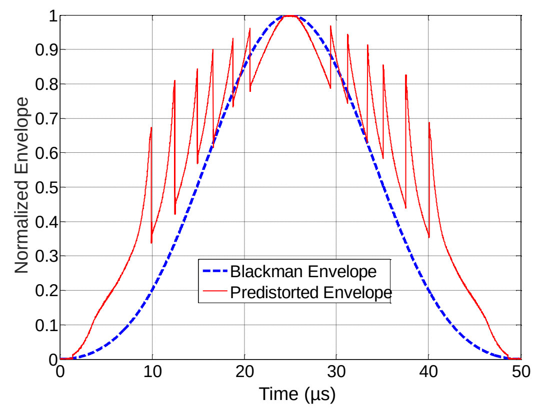

Fig. 11. Comparison between the ideal envelope of the RF input signal and the actual pre-distorted one for the case of pulse shaping with Blackman window.

By observing results in Figs. 8, 9, 10 and 11, it is seen that the PA output magnitude (thus power and gain) significantly changes with supply level, showing a strong nonlinear behavior of the PA. This indicates that the operating regime cannot be defined as pure envelope tracking, since its fundamental definition, given for example in [26], requires that the PA operates almost linearly under supply variation. Since the amplitude sensitivity to supply variation is not 1:1 (see Fig. 10 and 11) the PA is also not operating in EER regime, but rather in a hybrid mode of supply modulation (SM) that maximizes efficiency, while the strong linearity is recovered by DPD.

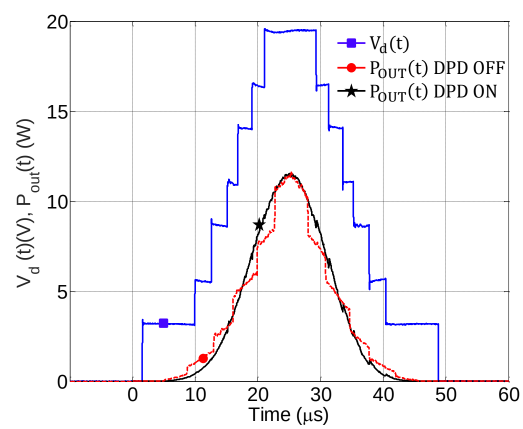

Fig. 12. Measured dynamic supply voltage $V_d(t)$ (blue square) and PA instantaneous output power $P_{out}(t)$ for SM operation with Blackman window pulse shaping with DPD OFF (red dot) and DPD ON (black star): gain steps due to the pDAC discrete operation are evident in the instantaneous output power when DPD is OFF, while they are compensated when DPD is applied.

V. Transmitter System Tests

The setup of Fig. 3 is used to compare the transmitter performance with different RF pulse shapes and supply modulation regimes. In the standard regime, both the RF envelope and supply voltage are unmodulated rectangular pulses (RR regime of Fig. 2a). Three different windowing functions, triangular, Hanning and Blackman, are applied to the RF pulse envelope, each one with two different pulsed-supply regimes: rectangular supply pulse (PS regime in Fig. 2a) and modulated drain supply (PS+SM regime in Fig. 2b). In the case of PS+SM regime, experiments with and without DPD are also performed and compared. The pulse duration for all the measurements presented in this section is τ = 50 μs, with 10% duty cycle.

The measured $V_d(t)$ when operating in PS+SM regime with a Blackman window is shown in Fig. 12, along with the PA RF output power. From these measurements, it is obvious that the memoryless polynomial open-loop DPD is effective in linearizing the PA nonlinearity that arises from discretized supply modulation. In Fig. 12, the smooth transitions between the levels in the pulse indicate excellent time alignment between the supply and RF paths achieved during the calibration phase. As observed in [10], a precise time alignment is more important in such a hybrid ET/EER system than in a pure ET transmitter.

Moreover, the voltage ringing associated with transitions in the $V_d(t)$ trace of Fig. 12 and the corresponding transients in the output envelope ($P_{OUT}(t)$) are limited in amplitude and duration due to the excellent switching characteristics of the selected GaN-on-Si technology (very low parasitics, see [24]) and the optimization of the connection between the pDAC and the PA.

In order to test spectral confinement, Fig. 13 and 14 show the measured output spectra of the three pulse shaping regimes with different windowing. In each plot of Fig. 14, the output spectrum in SM regime with DPD (RX, bold solid line) is compared with the ideal spectrum of that particular windowing (TX, dashed bold line). The measured spectrum in the conventional RR regime (Rectangular, dashed thin line) is also shown for reference.

Finally, in Fig. 13, the spectra obtained with RF pulse shaping and no DPD are compared to the rectangular constant-supply pulse case (PS regime of Fig. 2a) and ideal spectra of the corresponding windowing. Even though in this regime the PA operates in strong backoff over most of the pulse duration, the output spectrum is distorted with respect to the ideal one, due to the nonlinearity of the PA towards the peak of the pulse, which increases the sideband level or shifts their position closer to the main lobe. Fig. 14 shows clearly the improvement when DPD is performed, with sidelobes spectra much closer to the ideal ones even in presence of the more nonlinear and efficient SM regime.

In Table I, the measured performance of the transmitter in the different regimes is compared and summarized. For each regime, the efficiencies of the PA and pDAC are stated separately, along with the total composite efficiency, averaged over the pulse duration in each case. As expected, the maximum PA PAE = 65% is obtained for constant-envelope rectangular pulses when the PA is always in saturation and operating at peak efficiency. However, in this case the first spectral sideband is at a high value of -12.8 dBc. With RF pulse shaping alone, and no supply modulation, the PAE drops to 40.2% for Hanning windowing. The application of pulse shaping in conjunction with SM provided by the pDAC, restores the PAE to 59.3%, providing an improvement of +19.1 PAE points with an associated improvement in suppression of the first spectral sidelobe of 18.7 dB. Similar improvements are observed for the triangular and Blackman pulse shapes, as summarized in the table.

TABLE I
PERFORMANCE WITH DIFFERENT PULSE SHAPING STRATEGIES

Pulse Shape Window (PAPR)	Bias supply Modulation	1st sidelobe (dBm)	Power per pulse W (dBm)	PAE (%) PA	p-DAC	tot.
Rectangular	Rectangular pulse	-12.8 dB	11.75 (40.7)	65.0	96	62.4
Blackman (5.17 dB)	Rectangular pulse	-30.2 dB	3.57 (35.52)	37.2	96	35.7
Blackman (5.17 dB)	SM + DPD	-46.0 dB (ideal -58 dB)	3.57 (35.52)	**58.1**	95	55.2
Triangle (4.77 dB)	Rectangular pulse	-28 dB *	3.91 (35.91)	35.1	96	33.4
Triangle (4.77 dB)	SM + DPD	-26.5 dB (ideal -26.5 dB)	3.91 (35.91)	**58.9**	95	55.9
Hanning (4.20 dB)	Rectangular pulse	-24.4 dB	4.40 (36.43)	40.2	96	38.6
Hanning (4.20 dB)	SM+ DPD	-31.5 dB (ideal -31.5 dB)	4.40 (36.43)	**59.3**	95	56.3

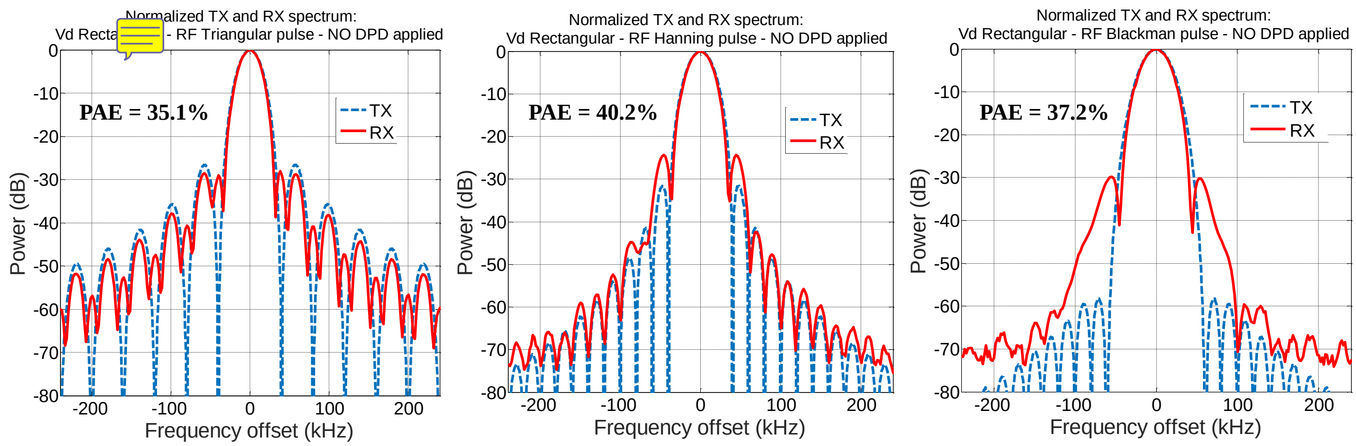

Fig. 13. PA measured output spectrum (RX) compared to the ideal one (TX) in pulse shaping regimes with unmodulated rectangular supply pulse.

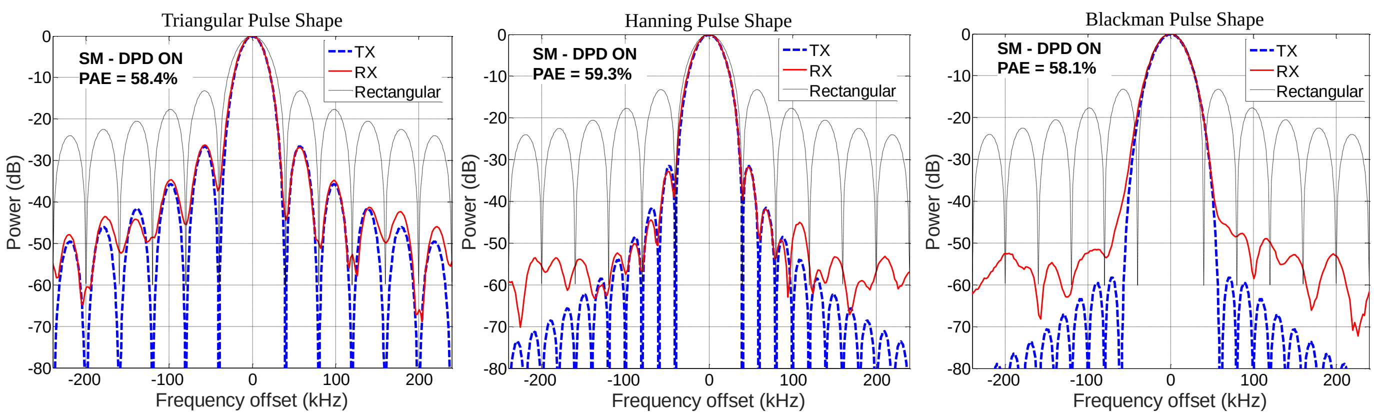

Fig. 14. Comparison between input (TX, i.e. ideal) and output spectra (RX) of the PA with triangular (left), Hanning (center) and Blackman (right) pulse shaping in SM regime with the pDAC and DPD applied. The rectangular (RR regime) pulse response is shown for comparison.

The very high efficiency provided by the pDAC working as a supply modulator (95%) guarantees that this advantage in terms of PAE of the RF PA is preserved also at the transmitter level, as seen in the last column in Table I.

VI. DISCUSSION AND CLUSIONS

This section discusses some properties of the SM PA system with a pDAC, such as additional functionality to include pulse-to-pulse shaping, as well as possible extensions of the DPD.

A. Pulse-to-Pulse Modulation

In ~~[14-16]~~, a resonant pulse modulator is presented with good efficiency, but with very limited pulse shape variation. In contrast, the approach described in this paper is completely flexible in terms of pulse shape and dynamic range. The $V_d(t)$ trajectory synthesized by the pDAC automatically adapts to the RF pulse shape and amplitude, according to the supply shaping function stored in the FPGA, delivering the radar pulse with the maximum possible efficiency compatible with the V_d range discretization.

It is sometimes advantageous from a system perspective to generate pulse sequences with pulse-to-pulse modulation. Two examples that demonstrate the flexibility are measured using the pDAC supply modulator and shown in Figs. 15 and 16. In the first case, a sequence of 4 pulses with different shapes, lengths and peak amplitudes is generated and in Fig. 15, the normalized envelopes of the pulse sequence are shown at the PA input and output, along with the corresponding $V_d(t)$ synthesized by the pDAC. The different types of shapes and values of length and peak power of the pulses are indicated in the inset of the figure. For each pulse, the setup automatically selects the $V_d(t)$ trajectory that maximizes the PA PAE.

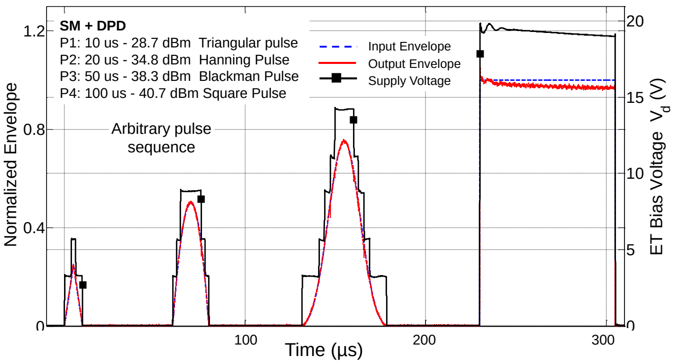

Fig. 15. Arbitrary pulse sequence: triangular, Hanning, Blackman and square pulse envelopes. The transmitted RF envelope is almost indistinguishable from the input one, due to the DPD correction effect. The corresponding dynamic supply voltage is also shown.

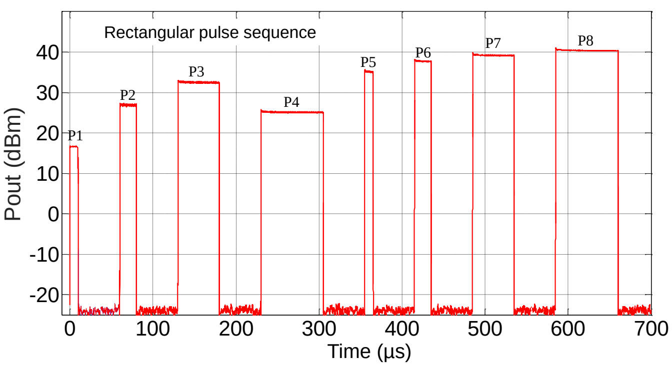

Fig. 16. Instantaneous PA output power for an arbitrary rectangular pulse sequence. Each power level is obtained with an optimal V_d for PAE maximization. No RF power (*Pout*) is present between pulses. The noise floor of the instrument is -25 dBm, when set with reference level and resolution bandwidth for the detection of the pulses with power up to 40 dBm.

TABLE II
PERFORMANCE WITH DIFFERENT RECTANGULAR PULSE AMPLITUDES

Pulse	Width (µs)	Supply Level (V)	Pout (dBm/W)	PAE (%) SM	PAE (%) pulsed Vd = 0-20V
P1	10	3.2	17 / 0.05	5	1
P2	20	5.6	27 / 0.5	27	9
P3	50	8.8	32.5 / 1.78	43	21
P4	75	11.2	35.3 / 3.38	55	32
P5	10	11.2	35.3 / 3.38	55	32
P6	20	14.4	37.6 / 5.75	60	45
P7	50	16.8	39.2 / 8.32	63	55
P8	75	20.0	40.5 / 11.22	66	66

Fig. 16 shows a different case of pulse-to-pulse modulation which could be used to modify time-on-target and power on target of a radar on a pulse-to-pulse basis. The pDAC can produce square voltage pulses with the seven different amplitudes described in (1), since V_{out} = 0 V is not used. Table II summarizes the pulse characteristics and the measured PAE and compares them with the performance obtained with constant 0-20 V supply pulses. The advantage in terms of PAE is substantial, since the PA *Vd* is practically optimized for all the different output power levels ranging from 17 dBm to 40.5 dBm.

B. Digital Pre-Distortion Extensions

It is worth noting that further improvements in linearization are possible. Some of the distortion is likely due to observed asymmetries between the upside and downside slopes of the shaped RF pulses, not corrected by the current DPD. This is most probably due to nonlinear trapping effects. We recently demonstrated a double-pulsed technique specifically designed for trapping effect characterization, which shows that memory effects due to trapping can be corrected with appropriate DPD. More details are given in [27].

As described in detail in [24], one of the main characteristics of the pDAC is that, despite being a switching converter, it does not use PWM modulation. This means that a fixed switching frequency is not used, but rather the commutation of the power switches is determined by the instantaneous amplitude of the envelope and by the quantization thresholds. In other words, the switching is adapting to the signal. This allows a minimum switching rate and thus high efficiency. As described in [24], for a periodic full-amplitude signal (*i.e.* full-amplitude radar pulse for this application) the power switches of the most significant bit commutate one time per period, the switches of the intermediate bit 3 times per period, and the switches of the least significant bit 7 ~~time~~ per period. Since the pulse repetition frequency of the tested radar signals 500 µs, the commutation frequencies of the power switches are 2, 6 and 14 kHz, respectively. Note that all these contributions, and several of their harmonics, fall within the measurement span of 250 kHz of Fig. 14. Thus, the main contributions of the switching spurious noise of the pDAC are included in the measurement span of Fig. 14 and appear to be negligible.

As previously observed in the comments of Fig. 12, the transition between voltage levels of the pDAC introduces additional distortion (envelope transients at the PA output). DPD with additional LUTs, specifically designed for compensation of switched supply voltage transients, was demonstrated in [28] to improve the spectral properties in such cases, and can be implemented in the FPGA pre-distorter in a straightforward manner. Further improvement of the linearity of the output spectra is expected, especially for pulse shapes with demanding characteristics (i.e. very high side-lobe suppression), for example Gaussian pulses with a high PAR, in addition to the Hanning and Blackman pulses in Fig. 14.

C. Summary

In summary, the application of a 3-bit pDAC as a supply modulator for radar pulse shaping is demonstrated for the first time. The approach is shown to give very high flexibility and state-of-the-art performance in terms of transmitter composite power-added efficiency (55%) with low spectral out-of-band regrowth. The GaN MMIC PA used in the transmitter demonstrates state-of-the-art performance with 65% peak efficiency at X band for 12 W output power and with >20 gain at 2-3 dB gain compression. The pDAC implemented with of-the-shelf GaN on Si devices operates at a very high efficiency of 95-96% efficiency.

Spectral confinement of radar signals with improved efficiency was tested for different RF pulse shape windowing and detailed comparisons with unmodulated pulsed regimes with a basic pulsed bias supply are presented. The improvement in spectral properties is enabled by pulse shaping combined with appropriate DPD.

In this work, we considered only amplitude modulation but it is possible to add both linear and non-linear frequency chirp as is shown in [1[illegible] Due to the capability of the VST to generate arbitrary digitally modulated baseband signals, with some modification of the firmware, the set up can be programmed for the test of the transmitter with both AM and FM modulated (i.e. chirped) driving signals.

The capability of the supply modulator to synthesize arbitrary supply trajectories with efficiency greater than 95% and the adopted DPD strategy result in a very high flexibility in the implementation of arbitrary pulse sequences with variable sequence order, pulse shape, length and peak amplitude, for advanced radar transmitters.

Acknowledgments

The authors would like to thank National Instruments for invaluable support with instrumentation and support, especially Dr. Truchard, Fabio Signorini, Dr. Marc Vanden Bossche, Patrick Webb and Dr. Takao Inoue. We also thank Qorvo for collaboration during MMIC fabrication, and [illegible]ling by the Office of Naval Research under the Defense Advanced Research Projects Agency (DARPA) Microscale Power Conversion (MPC) Program (N00014-11-1-0931) at the University of Colorado, Boulder. Tommaso Cappello acknowledges support through a graduate fellowship at the DEI Department of the University of Bologna.

References

[1] M. I. Skolnik, Radar Handbook, New York, NY: McGraw-Hill, 2008, Ch.11.

[2] G. van der Bent, P. de Hek, S. Geurts, Member, A. Telli, H. Brouzes, M. Besselink, [illegible]van Vliet, "A 10 Watt S-Band MMIC Power Amplifier With Integ[illegible] 100 MHz Switch-Mode Power Supply and Control Circuitry for Active Electronically Scanned Arrays," *IEEE Journal ~~Of~~ Solid-State Circuits*, vol. 48, ~~No.~~ 10, pp. 2285-2295, October 2013.

[3] D.A. Garren, M.K. Osborn, A.C Odom, J.S. Goldstein, S.U. Pillai, [illegible] Guerci, "Enhanced target detection and identification via optimis[illegible] radar transmission pulse shape", *IEE Proceedings of Radar, Sonar and Navigation*, vol. 148, ~~Iss.~~ 3, pp. 130-138, 2001.

[4] Committee on Weather Radar Technology Beyond NEXRAD, Board on Atmospheric Sciences and Climate, Division on Earth and Life Studies, National Research Council, "Weather Radar Technology Beyond NEXRAD," 2002, National Academy Press, Washington, D.C, USA.

[5] C. Baylis, M. Fellows, L. Cohen, R. Marks, "Solving the spectrum crisis: Intelligent, reconfigurable microwave transmitter amplifiers for cognitive radar," *IEEE Microwave Mag*azine, vol. 15, no. 5, pp. 94–107, July 2014.

[6] R. Chen, [illegible]antrell, "Highly bandlimited radar signals," *Proceedings of the IEEE [illegible]r Conference*, pp. 220–226, 2002.

[7] J. de Graaf, H. Faust, J. Alatishe, and S. Talapatra, "Generation of spectrally confined transmitted radar waveforms: Experimental results," in ~~2006~~ *IEEE Conference on Radar*, pp. 76–83, Apr. 2006.

[8] E. McCune, *Dynamic power supply transmitters*, Cambridge University Press, 2015, Chapters 5, 6.

[9] G. Hanington, P. Asbeck, L. Larson, "High-efficiency power amplifier using dynamic power-supply voltage for CDMA applications," *IEEE Trans. on Microwave Theory and Techniques*, vol. 47, no. 8, pp. 1471–1476, Aug. 1999.

[10] F. Wang, A. H. Yang, D. F. Kimball, L. E. Larson, P. M. Asbeck, "Design of wide-bandwidth envelope-tracking power amplifiers for OFDM applications," *IEEE Trans. on Microwave Theory and Techniques*, vol. 53, no. 4, pp. 1244–1255, April 2005.

[11] D. F. Kimball, J. Jeong, E. C. Hsia, P. Draxler, S. Lanfranco, W. Nagy, K. Linthicum, L. E. Larson, P. M. Asbeck, "High-Efficiency Envelope-Tracking W-CDMA Base-Station Amplifier Using GaN HFETs," *IEEE Trans. on Microwave Theory and Techniques*, vol. 54, no. 11, pp. 3848–3856, Nov. 2006.

[12] J. Hoversten, S. Schafer, M. Roberg, M. Norris, D. Maksimovic, Z. Popovic, "Codesign of PA, Supply, and Signal Processing for Linear Supply-Modulated RF Transmitters," *IEEE Trans. on Microwave Theory and Techniques*, vol. 60, issue 6, Part 2, pp. 2010 – 2020, June 2012.

[13] K. Bumman, M. Junghwan, K. Ildu, "Efficiently amplified," *Microwave Magazine*, IEEE, vol. 11, no. 5, pp. 87 –100, Aug. 2010.

[14] M. Roberg, M. Rodriguez, D. Maksimovic, [illegible]opovic, "Efficient and Linear Amplification of Spectrally Confined [illegible]d AM Radar Signals," *IEEE Microwave and Wireless Components Letters*, vol. 22, Iss. 6, pp. 279 – 281, June 2012.

[15] M. Rodriguez, M. Roberg, A. Zai, E. Alarcon, Z. Popovic, D. Maksimovic, "Resonant Pulse-Shaping Power Supply for Radar Transmitters", *IEEE Trans. on Power Electronics*, vol. 29, no. 2, pp. 707-718, Feb. 2014.

[16] Zai, A.; Pinto, M.; Coffey[illegible] Popovic, Z., "Supply-Modulated Radar Transmitters With Amplitude-Modulated Pulses," in *IEEE Trans. on Microwave Theory and Tec*[illegible]l.63, no. 9, pp. 2953-2964, Sept. 2015.

[17] L. Kahn, "Single-sideband transmission by envelope elimination and restoration," Proc. of the IRE, vol. 40, no. 7, pp. 803 –806, July 1952.

[18] C. Florian, R.P. Paganelli, J.A. Lonac, "12-W X-Band MMIC HPA and Driver Amplifiers in InGaP-GaAs HBT Technology for Space SAR T/R Modules," *IEEE Trans. On Microwave Theory And Techniques*, vol. 60, issue 6, part 2, pp. 1805 – 1816, June 2012.

[19] C. Florian, R. Cignani, D. Niessen, A. Santarelli, "A C-Band AlGaN-GaN MMIC HPA for SAR," *IEEE Microwave and Wireless Components Letters*, vol. 22, issue 9, pp. 471–473, Sep. 2012.

[20] C. Florian, R. Cignani, A. Santarelli, F. Filicori, "Design of 40-W AlGaN/GaN MMIC high power amplifiers for C-Band SAR applications," *IEEE Trans. on Microwave Theory and Techniques*, vol. 61, issue 12, pp. 4492-4504, Dec. 2013.

[21] P. A. Godoy, S. Chung, T. W. Barton, D. J. Perreault, J. L. Dawson, "A highly efficient 1.95-GHz, 18-W asymmetric multilevel outphasing transmitter for wideband applications," in *IEEE MTT-S International Microwave Symposium*, pp. 1–4, June 2011.

[22] P. A. Godoy, S. Chung, T. W. Barton, D. J. Perreault, J. L. Dawson, "A 2.4-GHz, 27-dBm Asymmetric Multilevel Outphasing Power Amplifier in 65-nm CMOS," *IEEE Journal of Solid-State Circuits*, vol. 47, no. 10, pp. 2372–2384, Oct. 2012.

[23] J. Hur, O. Lee, K. Kim, K. Lim, and J. Laskar, "Highly efficient uneven multi-level LINC transmitter," *Electronics Letters*, vol. 45, no. 16, p. 837, July 2009.

[24] C. Florian, T. Cappello, R.P. Paganelli, D. Niessen, F. Filicori, "Envelope Tracking of an RF High Power Amplifier With an 8-Level Digitally Controlled GaN-on-Si Supply Modulator", *IEEE Trans. on Microwave Theory and Techniques*, vol. 63, issue 8, pp. 2589-2602, Aug. 2015.

[25] A. Zai, Li Dongxue, S. Schafer, Z. Popovic, "High-efficiency X-band MMIC GaN power amplifiers with supply modulation," in *IEEE MTT-S International Microwave Symposium*, pp. 1-4, June 2014.

[26] F.H. Raab, P. Asbeck, S. Cripps, P.B. Kenington, Z.B. Popovic, N. Pothecary, J.F. Sevic, N.O. Sokal, "Power amplifiers and transmitters for RF and microwave," IEEE Trans. on Microwave Theory and Tech., Vol. 50 , No. 3, March 2002, pp. 814 – 826.

[27] C. Florian, D. Niessen, T. Cappello, A. Santarelli, F. Filicori, Z. Popovic, *"Pre-Pulsing Characterization of GaN Pas with Dynamic Supply," accepted for publication in IEEE MTT-S International Microwave Symp*[illegible] San Francisco, USA, May 2016.

[28] N. Wolff, W. He[illegible]h, O. Bengtsson, "A Novel Model for Digital Predistortion of Discrete Level Supply-Modulated RF Power Amplifiers," *IEEE Microwave and Wireless Components Letters*, vol. 26, issue 2, pp. 146-148.